The Astrophysical Journal, 835:245 (5pp), 2017 February 1 doi:10.3847/1538-4357/835/2/245

Development of Turbulent Magnetic Reconnection in a Magnetic Island

Can Huang[1,2], Quanming Lu[1,2], Rongsheng Wang[1,2], Fan Guo[3], Mingyu Wu[1,2], San Lu[1,2], and Shui Wang[1,2]
[1] CAS Key Laboratory of Geospace Environment, Department of Geophysics and Planetary Science, University of Science and Technology of China, Hefei 230026, China; qmlu@ustc.edu.cn
[2] Collaborative Innovation Center of Astronautical Science and Technology, China
[3] Theoretical Division, Los Alamos National Laboratory, Los Alamos, NM 87545, USA
Received 2016 May 8; revised 2016 December 5; accepted 2017 January 5; published 2017 February 1

Abstract

In this paper, with two-dimensional particle-in-cell simulations, we report that the electron Kelvin–Helmholtz instability is unstable in the current layer associated with a large-scale magnetic island, which is formed in multiple X-line guide field reconnections. The current sheet is fragmented into many small current sheets with widths down to the order of the electron inertial length. Secondary magnetic reconnection then occurs in these fragmented current sheets, which leads to a turbulent state. The electrons are highly energized in such a process.

Key words: acceleration of particles – magnetic reconnection – Sun: flares

1. Introduction

In magnetic reconnection, magnetic field lines with opposite directions approach each other and reconnect in a current sheet, where a magnetic X-line configuration is formed, and the newly reconnected field lines are expanded away from the X line (Parker 1957; Sweet 1958). The essence of magnetic reconnection is to convert magnetic energy into plasma kinetic energy, and many explosive phenomena in space and astrophysical plasmas, such as solar flares (Giovanelli 1946; Masuda et al. 1994), flares on strongly magnetized neutron stars (Aly & Kuijpers 1990), and substorms in the Earth's magnetosphere (Nagai et al. 1998; Angelopoulos et al. 2008), are considered to be related to magnetic reconnection. The generation of magnetic islands is usually accompanied in such a process by a topological change of magnetic field lines (Wang et al. 2010; Daughton et al. 2011; Dong et al. 2012), and their roles in magnetic reconnection have recently been paid more and more attention. Magnetic islands can enhance not only the reconnection rate (Daughton et al. 2006; Bhattacharjee et al. 2009) but also the efficiency of particle acceleration (Drake et al. 2006a; Fu et al. 2006; Chen et al. 2008; Guo et al. 2014; Takasao et al. 2016). Plasma particles can gain energy as they are reflected from two ends of a contracting magnetic island (Drake et al. 2006a; Fu et al. 2006). The interactions of magnetic islands can enhance the reconnection rate (Daughton et al. 2006; Bhattacharjee et al. 2009) and also energize particles (Pritchett 2007; Oka et al. 2010; Tanaka et al. 2011; Song et al. 2012; Zank et al. 2014; Wang et al. 2016a). The interactions of magnetic islands in the diffusion region have been evidenced by in situ observations (Wang et al., 2016b).

Magnetic islands may be generated via the plasmoid instability in either a Sweet–Parker current sheet with a sufficiently large Lundquist number (Biskamp 1986; Lapenta 2008; Samtaney et al. 2009; Huang & Bhattacharjee 2010; Comisso et al. 2013) or an extended electron current sheet around an X line (Daughton et al. 2006, 2009; Drake et al. 2006b; Dorfman et al. 2012; Fermo et al. 2012); therefore, their sizes can range from a magnetohydrodynamic (MHD) up to an electron inertial scale. Particle-in-cell (PIC) simulations of antiparallel reconnection have shown that the Weibel instability may be unstable inside a formed magnetic island with the size of several ion inertial lengths (Lu et al. 2011; Schoeffler et al. 2013). However, until now, the kinetic characteristics of a large-scale magnetic island have not been investigated. Here, for the first time, by performing two-dimensional (2D) PIC simulations of guide field magnetic reconnection, we found that the electron Kelvin–Helmholtz instability is unstable in a large-scale magnetic island, and the associated current layer is then fragmented into many small current sheets with different sizes. Secondary magnetic reconnection is induced in these small current sheets, which at last leads to a turbulent state of reconnection.

The paper is organized as follows. The simulation model is described in Section 2, and the simulation results are presented in Section 3. In Section 4, we discuss and summarize the results.

2. Simulation Model

Our PIC simulations, which solve the relativistic Vlasov–Maxwell system of equations, start from a Harris current sheet equilibrium with magnetic field $\boldsymbol{B}(z) = B_0 \tanh(z/\delta)\boldsymbol{e}_x + B_{y0}\boldsymbol{e}_y$, where B_0 is the asymptotic magnetic field, and $B_{y0} = B_0$ is the uniform guide field. The particle number density is $n(z) = n_b + n_0 \operatorname{sech}^2(z/\delta)$, where $n_b = 0.1n_0$ represents the background density. The half-width of the current sheet is $\delta = 0.75d_i$, and d_i is the ion inertial length based on n_0. Both ions and electrons are assumed to have Maxwellian velocity distributions, with an initial temperature ratio $T_{i0}/T_{e0} = 5$ and a mass ratio $m_i/m_e = 100$, where the subscripts i and e stand for ion and electron, respectively. The light speed is assumed to be $c = 15V_A$, where V_A is the Alfvén speed based on B_0 and n_0. The plasma beta in the inflow region is $\beta_i = 2\mu_0 p_{bi}/B_0^2 \approx 0.083$ and $\beta_e = 2\mu_0 p_{be}/B_0^2 \approx 0.017$, which is typical in the solar corona or solar wind. The electromagnetic fields are defined on the grids and updated by integrating the Maxwell equations with an explicit leapfrog scheme, while the ions and electrons are treated as individual particles and advanced in these electromagnetic fields. The simulation is performed in the (x, z) plane, and a large-scale computational domain $[-L_x/2, L_x/2] \times [-L_z/2, L_z/2]$ with $L_x = 300d_i$ and $L_z = 50d_i$ is used here. The grid size is $\Delta x = \Delta y = 0.025d_i$. More than 10^{10} particles for each species are employed in the simulation. Periodic boundary conditions are assumed in the x direction, while in the z direction conducting

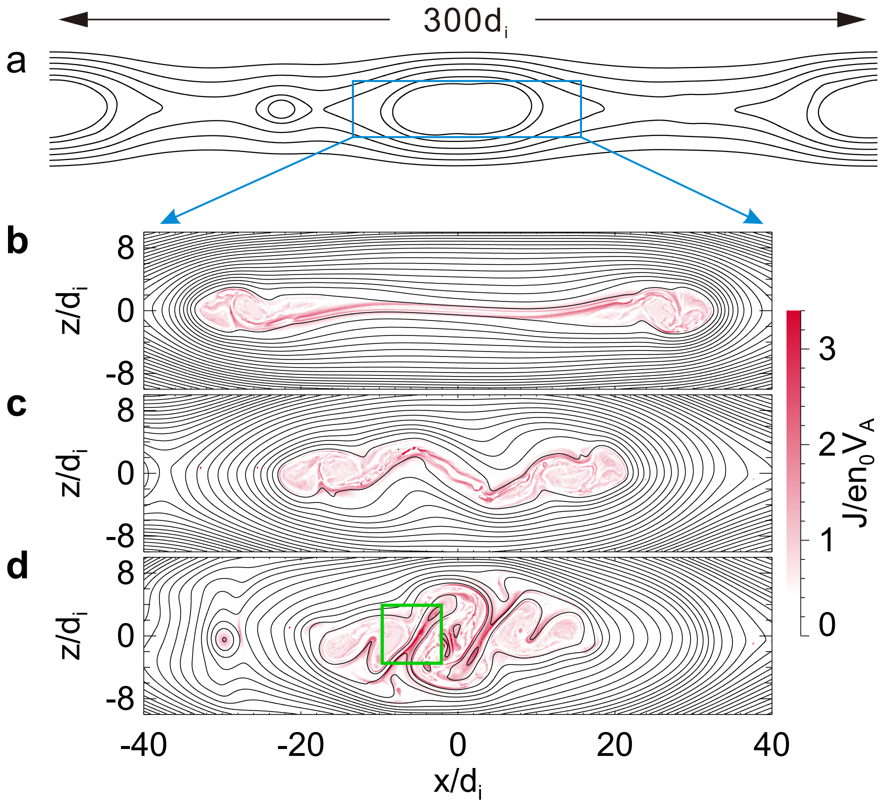

Figure 1. Time evolution of the total current density J in the large-scale magnetic island: (a) schematic diagram of magnetic field lines during the magnetic reconnection, and the evolution of the total current density J with superimposed magnetic field lines at $\Omega_i t =$ (b) 69, (c) 79, and (d) 89.5.

boundary conditions are retained, and particles are specularly reflected at the boundaries. The reconnection is initiated by two small, local flux perturbations centered at $x = -80$ and $x = 80$.

3. Simulation Results

The reconnection begins at about $\Omega_i t = 20$, and then a large island with a length of about $100\, d_i$ is formed in the center of the simulation domain. Figure 1 shows the time evolution of the total current density $J/en_0 V_A$ in the magnetic island. Although the size and outermost layer of the magnetic island show almost no change, its inner part is twisted, and a fragmented current layer is generated. Such a twisted current is formed due to the electron Kelvin–Helmholtz instability, which is excited by the super-Alfvenic electron shear flow. This can be demonstrated by Figure 2, which shows (a) the electron bulk velocity along the x direction V_{ex}, and (b) the profiles of the electron bulk velocity V_{ex} and the local electron Alfvén speed $|V_{Aex}|/2$ along the x direction at $\Omega_i t = 75$, when the electron Kelvin–Helmholtz instability just begins to be excited. The super-Alfvenic electron shear flow can be obviously observed, and such an electron flow is caused by the $\boldsymbol{E} \times \boldsymbol{B}$ drift, as demonstrated in Huang et al. (2015). The characteristic growth rate must exceed the whistler frequency so that the electron Kelvin–Helmholtz instability is unstable in an electron current sheet. The stability threshold is the change of the electron bulk velocity $\Delta V_{ex} > |V_{Aex}|/2$ (Fermo et al. 2012). From the shadow region of the figure, we can find that the change of the electron bulk velocity is $\Delta V_{ex} \sim 2|V_{Aex}|$, which exceeds the stability threshold of the electron Kelvin–Helmholtz instability. Therefore, the electron Kelvin–Helmholtz instability is unstable in the large-scale magnetic island. Many small current sheets with widths down to the electron inertial length, which are embedded in the current layer associated with the inner part of the magnetic island, are then formed due to the excitation of the electron Kelvin–Helmholtz instability. The current density in these small current sheets can be enhanced by about two to three times that of the nearby regions, and the magnetic field lines are highly twisted and stretched.

An enlarged view of the evolution of such a small current sheet, which is denoted by the green box in Figure 1(d), is shown in Figure 3. In the figure, the left-hand panel plots the vector of electron flow and the current density along the y direction J_{ey}, while the right-hand panel shows the electron temperature T_e and magnetic field lines. With the thinning of the current sheet, the current density is dramatically enhanced, and the width can be squeezed to several electron inertial lengths. Then, magnetic reconnection occurs in the small current sheet, which is called secondary magnetic reconnection. High-speed electron flows are observed in the outflow region of secondary reconnection, and also the electrons are highly heated up to about $0.22 m_e c^2$ around the X line and in the outflow region.

In order to know how the magnetic energy is dissipated into the plasma kinetic energy during secondary magnetic reconnection, in Figure 4(a) we present the parallel electric field $E_{||}$, the electron-frame dissipation measure $D_e = \boldsymbol{J}_e \cdot (\boldsymbol{E} + \boldsymbol{V}_e \times \boldsymbol{B})$, and the electron temperature anisotropy $T_{e||}/T_{e\perp}$ in the green box in Figure 1(d). The electron-frame dissipation measure D_e is consistent with the definition used in Zenitani et al. (2011). We

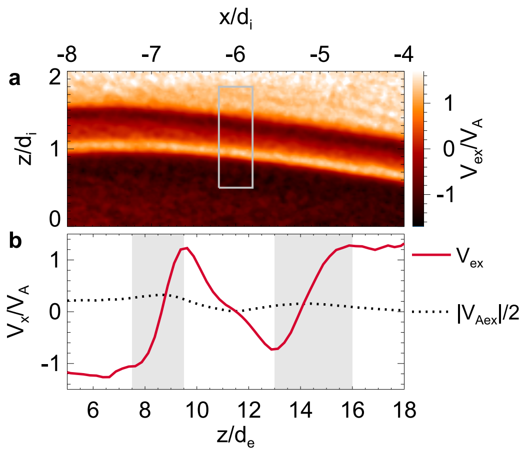

Figure 2. An enlarged view of (a) the electron bulk velocity along the x direction V_{ex} in the region $[-8d_i, -4d_i] \times [0, 2d_i]$, and (b) the profiles of the electron bulk velocity V_{ex} and the local electron Alfvén speed $|V_{Aex}|/2$ along the x direction at $\Omega_i t = 75$, when the electron Kelvin–Helmholtz instability just begins to be excited. The local electron Alfvén speed V_{Ae} is calculated based on the in-plane magnetic field.

can find that a strong parallel electric field exists around the X line of secondary reconnection, where the dissipation measure D_e has a large value. The magnetic energy is then dissipated into the plasma kinetic energy due to the existence of the parallel electric field around the X line, and the electrons are highly heated around the X line with a temperature anisotropy about $T_{e||}/T_{e\perp} \sim 10$. At the same time, we can also find the enhancement of energetic electrons around the X line, as shown in Figure 4(b), which plots the electron energy flux with kinetic energy higher than 0.1 $m_e c^2$. The superthermal electrons accelerated in secondary reconnection have a power-law spectrum, which can be observed in Figure 4(c). The power-law index of the nonthermal electrons is about $-5/3$. The electrons are accelerated mainly by the parallel electric field around the X line of secondary magnetic reconnection.

It is obvious that secondary magnetic reconnection can occur inside a large-scale magnetic island. A further detailed analysis shows that these small fragmented current sheets have different sizes, and then the secondary islands formed during secondary reconnection in these small current sheets also have different sizes. The spectra of the fluctuations of the magnetic field, electric field, and electron velocity at $\Omega_i t = 89.5$ are described in Figure 5. These spectra are obtained by Fourier transforming these values in the region marked with the blue box in Figure 1(a). Obviously, the spectra of these physical values satisfy a power law, and the index changes significantly around $kd_e \sim 1$. At the scale larger than $kd_e \sim 1$, the index is about $-3/2$, while at the scale smaller than $kd_e \sim 1$, the index is about $-7/3$. The reason for the steepness of the power spectra below the electron inertial length is that the dissipation of the magnetic energy due to secondary reconnection occurs in these small electron current sheets. Therefore, we can conclude that secondary reconnection induced in the large island is turbulent reconnection.

4. Conclusions and Discussion

A new scenario for the kinetic characteristics of a large-scale island can be illustrated in Figure 6. In such a twisted magnetic island, the associated current layer is fragmented into many small current sheets with different sizes. Secondary reconnection, which occurs in these small current sheets, furthers twist the large-scale island, which leads to the generation of small magnetic islands with different sizes and a turbulent state of magnetic reconnection. It is worth noting that in our simulations the resulting turbulent reconnection is limited to a 2D state. However, a turbulence in reality is fundamentally a three-dimensional process, which is qualitatively different from that of a 2D one and needs further investigation in the future.

The electrons can be accelerated between these small magnetic islands, which are generated inside the large-scale magnetic island. Therefore, in addition to the acceleration during the reflection at the two ends of a large-scale island (Drake et al. 2006a; Fu et al. 2006), the electrons can also be highly accelerated during the secondary reconnection induced in the large-scale island. This will improve our understanding of electron acceleration in magnetic reconnection: energetic electrons should fill a large-scale island. It may explain the observations of particle acceleration

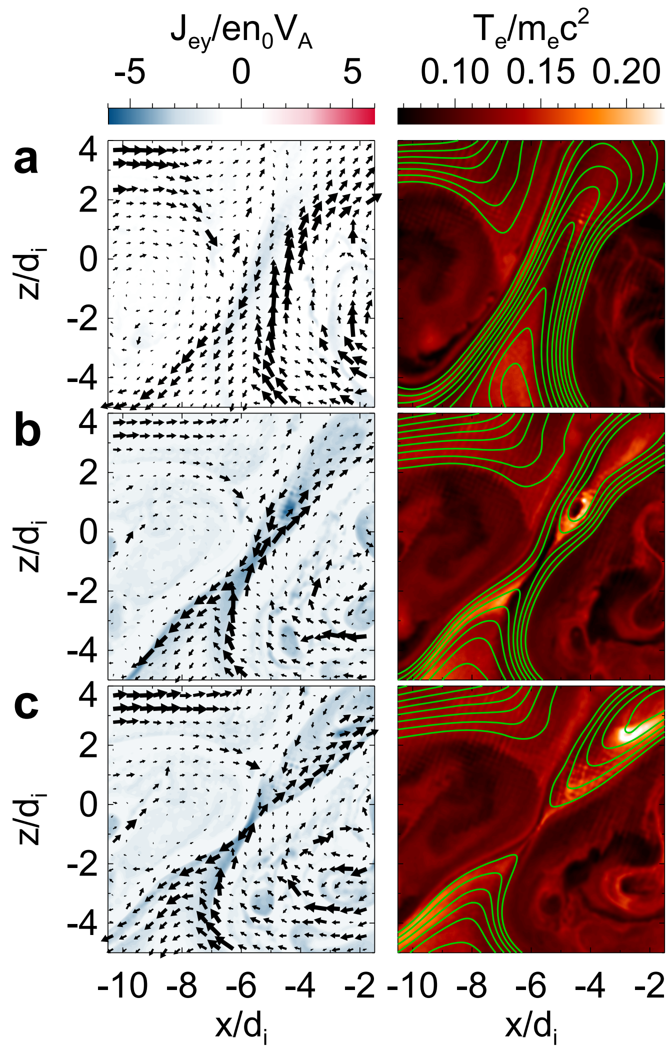

Figure 3. Snapshots of out-of-plane electron current density J_{ey} (left panel) and electron temperature T_e (right panel) in the large-scale magnetic island (the green box in Figure 1(d)) at $\Omega_i t =$ (a) 87, (b) 89.5, and (c) 90.5. The arrows and green curves represent the vectors of electron flow and in-plane magnetic field lines, respectively.

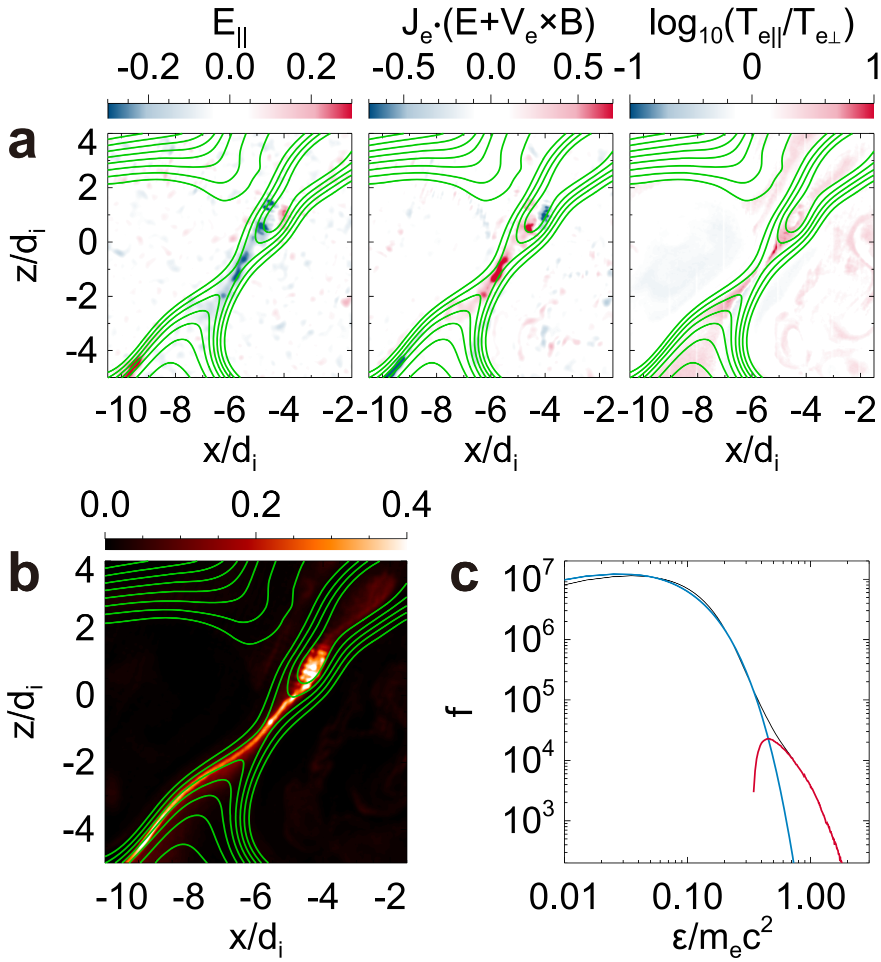

Figure 4. Energy dissipation and production of high-energy electrons during secondary reconnection. (a) The parallel electric field $E_{||}$ (normalized by $V_A B_0$), the electron-frame dissipation $\boldsymbol{J}_e \cdot (\boldsymbol{E} + \boldsymbol{V}_e \times \boldsymbol{B})$ (normalized by $n_0 m_i V_A^2 \Omega_i$), and the electron temperature anisotropy $T_{e||}/T_{e\perp}$. (b) The energy flux (normalized by $n_0 m_e c^2$) of the electrons with kinetic energy $\varepsilon > 0.1\ m_e c^2$. (c) The electron energy spectrum (the vertical axis shows the counts). In (c), the black curve is plotted according to the data from the simulation, while the blue curve is the Gaussian fitting of the data $0.01 \leqslant \varepsilon/m_e c^2 \leqslant 0.07$, and the red curve shows the nonthermal population. The data are obtained at $\Omega_i t = 89.5$ from the region denoted by the green box in Figure 1(d).

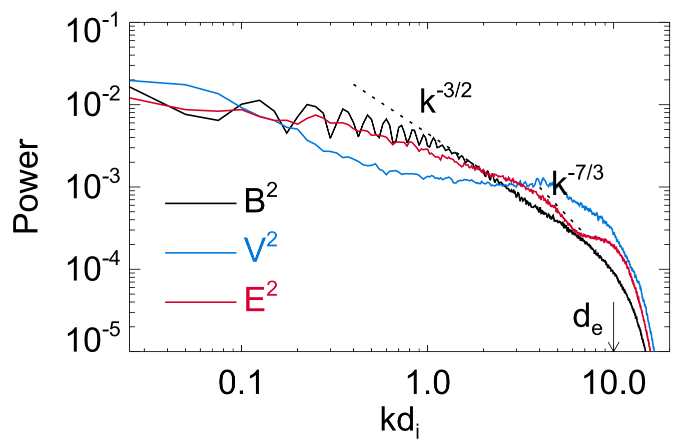

Figure 5. Cascade of turbulent reconnection in the large-scale magnetic island. The power spectra of the magnetic fields (black curve, normalized by B_0^2), the electron flows (blue curve, normalized by V_A^2), and the electric fields (red curve, normalized by $V_A^2 B_0^2$) are shown. The data are obtained within the magnetic island ($-20 \leqslant x/d_i \leqslant 20$ and $-10 \leqslant z/d_i \leqslant 10$) at $\Omega_i t = 89.5$.

associated with magnetic islands in the solar atmosphere (Takasao et al. 2016). By the way, secondary reconnection induced in a large-scale island provides another way to dissipate the magnetic energy into the plasma kinetic energy besides the diffusion region around the X line, and its evolution is much faster due to its small scale.

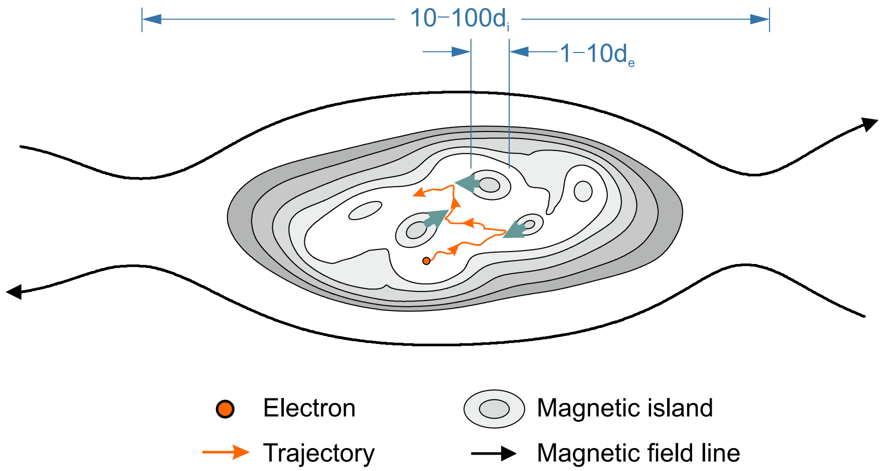

Figure 6. A multi-island geometry in a large-scale magnetic island. Diagram showing volume-filling microislands (on the scale of 1–10 d_e) produced by secondary reconnections within a large magnetic island (on the scale of 10–100 d_i). An energetic particle can be reflected between magnetic islands. Black lines show magnetic field lines, green arrows show the reconnection outflows with Alfvén speed, and the red line is the trajectory of the energetic particle.

This research was supported by the National Science Foundation of China, grant Nos. 41331067, 41527804, 11220101002, 11235009, 41121003, 973 Program (2013CBA01503), and Key Research Program of Frontier Sciences, CAS (QYZDJ-SSW-DQC010).

References

Aly, J. J., & Kuijpers, J. 1990, A&A, 227, 473
Angelopoulos, V., McFadden, J., Larson, D., et al. 2008, Sci, 321, 931
Bhattacharjee, A., Huang, Y. M., Yang, H., & Rogers, B. 2009, PhPl, 16, 112102
Biskamp, D. 1986, PhFl, 29, 1520
Chen, L. J., Bhattacharjee, A., Puhl-Quinn, P. A., et al. 2008, NatPh, 4, 19
Comisso, L., Grasso, D., Waelbroeck, F., & Borgogno, D. 2013, PhPl, 20, 092118
Daughton, W., Roytershteyn, V., Albright, B. J., et al. 2009, PhRvL, 103, 065004
Daughton, W., Roytershteyn, V., Karimabadi, H., et al. 2011, NatPh, 7, 539
Daughton, W., Scudder, J., & Karimabadi, H. 2006, PhPl, 13, 072101
Dong, Q. L., Wang, S. J., Lu, Q. M., et al. 2012, PhRvL, 108, 215001
Dorfman, S., Ji, H., Yamada, M., et al. 2012, GeoRL, 40, 233
Drake, J. F., Swisdak, M., Che, H., & Shay, M. A. 2006a, Natur, 443, 553
Drake, J. F., Swisdak, M., Schoeffler, K. M., Rogers, B. N., & Kobayashi, S. 2006b, GeoRL, 33, L13105
Fermo, R. L., Drake, J. F., & Swisdak, M. 2012, PhRvL, 108, 255005
Fu, X. R., Lu, Q. M., & Wang, S. 2006, PhPl, 13, 012309
Giovanelli, R. G. 1946, Natur, 158, 81
Guo, F., Li, H., Daughton, W., & Li, Y. H. 2014, PhRvL, 113, 155005
Huang, C., Lu, Q. M., Guo, F., et al. 2015, GeoRL, 42, 7282
Huang, Y. M., & Bhattacharjee, A. 2010, PhPl, 17, 062104
Lapenta, G. 2008, PhRvL, 100, 235001
Lu, S., Lu, Q. M., Shao, X., Yoon, P. H., & Wang, S. 2011, PhPl, 18, 072105
Masuda, S., Kosugi, T., Hara, H., Tsuneta, S., & Ogawara, Y. 1994, Natur, 371, 495
Nagai, T., Fujimoto, M., Saito, Y., et al. 1998, JGR, 103, 4419
Oka, M., Phan, T. D., Krucker, S., Fujimoto, M., & Shinohara, I. 2010, ApJ, 714, 915
Parker, E. N. 1957, JGR, 62, 509
Pritchett, P. L. 2007, PhPl, 14, 052102
Samtaney, R., Loureiro, N. F., Uzdensky, D. A., Schekochihin, A. A., & Cowley, S. C. 2009, PhRvL, 103, 105004
Schoeffler, K. M., Drake, J. F., Swisdak, M., & Knizhnik, K. 2013, ApJ, 764, 126
Song, H. Q., Chen, Y., Li, G., Kong, X. L., & Feng, S. W. 2012, PhRvX, 2, 022015
Sweet, P. A. 1958, in IAU Symp. 6, Electro-magnetic Phenomena in Cosmical Physics, ed. B. Lehnert (Cambridge: Cambridge Univ. Press), 123
Takasao, S., Asai, A., Isobe, H., & Shibata, K. 2016, ApJ, 828, 103
Tanaka, K. G., Fujimoto, M., Badman, S., & Shinohara, I. 2011, PhPl, 18, 022903
Wang, H. Y., Lu, Q. M., Huang, C., & Wang, S. 2016a, ApJ, 821, 84
Wang, R. S., Lu, Q. M., Du, A. M., & Wang, S. 2010, PhRvL, 104 175003
Wang, R. S., Lu, Q. M., & Nakamura, R. 2016b, NatPh, 12, 263
Zank, G. P., le Roux, J. A., Webb, G. M., Dosch, A., & Khabarova, O. 2014, ApJ, 797, 28
Zenitani, S., Hesse, M., Klimas, A., & Kuznetsova, M. 2011, PhRvL, 106, 195003